Research Article | Vol. 27, No. 3 | 4 Feb 2019 | OPTICS EXPRESS 3439
Optics EXPRESS

Large-area fabrication of microlens arrays by using self-pinning effects during the thermal reflow process

S. G. HEO,[1,2] D. JANG,[3] H.-J. KOO,[1,3] AND H. YOON[1,2,3,*]

[1]*Department of New Energy Engineering, Seoul National University of Science & Technology, Seoul 01811, South Korea*
[2]*3D EYES, 131-1 Second Business Incubation Center, 232 Gongeneung-ro, Nowon-gu, Seoul 01811, South Korea*
[3]*Department of Chemical and Biomolecular Engineering, Seoul National University of Science & Technology, Seoul 01811, South Korea*
**hsyoon@seoultech.ac.kr*

Abstract: Generally, the fabrication of curved structures such as microlens arrays has been regarded as an expensive and complicated process. Here, we propose a facile method to form a microlens array with controlled lens curvature by combining residue-free nanoimprint lithography (NIL) with V-shaped molds and the successive thermal reflow procedure of the printed polymeric structures. The V-shaped molds used in this study enable the bottom substrate to be exposed after the NIL process when the initial thickness is controlled. Then, we use the thermal reflow to realize hemi-cylindrical curved lenses by applying heat. The polymers are self-pinned on the exposed substrate, which is strong enough to fix the boundary to not dewet or be flattened in the broad temperature range of the reflow process, which is essential for a large-area fabrication. Furthermore, we demonstrate the modulation of the focal lengths of the lenses by controlling the initial polymer thickness coated on a substrate.

1. Introduction

Three-dimensional curved structures such as microlens arrays are widely used as important elements in the fields of optical communication and optoelectronics [1–4]. For example, lenticular lenses have been utilized to create 3D displays without the need for special glasses. While micromachining methods [5–9] are widely used for the fabrication of curved lens structures, the reflow process after the nanoimprinting technique has also been highlighted because it has advantage to obtain smooth round surfaces [10–16]. Nanoimprint lithography (NIL) is a microfabrication technology using templates to press polymeric resins and is widely used to form micropatterns for various applications, such as photonic crystals [17,18], cell-culturing substrates [19,20], thin film electronics [21,22], and optical devices [23,24]. Even though NIL is a simple and cost- effective process, it generally needs an additional process such as reactive etching (RIE) with oxygen gas [12–14,25–29] to remove residual layers of resist, which remains difficult due to the need for direct contact between the brittle molds and substrates [30,31]. It is also not suitable for a large-area fabrication because the plasma etching needs equipment operating in high vacuum, which is difficult to obtain commercially. In addition, post process such as additional hydrophobic treatment is necessary to pin the round pattern during thermal reflow because oxygen plasma for removing residual layers activates the substrate surface to spread the viscous polymer [12]. Here, we propose a facile method to fabricate curved structures such as lenticular lenses by using residue-free nanoimprint lithography with V-shaped molds followed by thermal reflow. When a substrate is exposed during NIL, the viscous polymers above the glass transition temperature (T_g) are self-pinned on the three-phase contact line between the polymer, air and the substrate without post hydrophobic treatments. The self-pinning effect on a substrate can enlarge the

#349778 https://doi.org/10.1364/OE.27.003439
Journal © 2019 Received 1 Nov 2018; revised 22 Dec 2018; accepted 27 Dec 2018; published 31 Jan 2019

Optics EXPRESS

temperature range for thermal reflow, which is essential for the large-area fabrication of curved lens arrays because the variation of the temperature within an equipment is inevitable. A V-shape mold has advantages for accomplishing a residue free NIL due to the localization of pressure to contact to a substrate directly, and minimizing the spacing between lenses. By varying the polymer thickness coated on the substrate, we could control the lens focal length, which can be estimated by using a simple model we established based on the mass balance of the polymer patterns.

2. Experimental

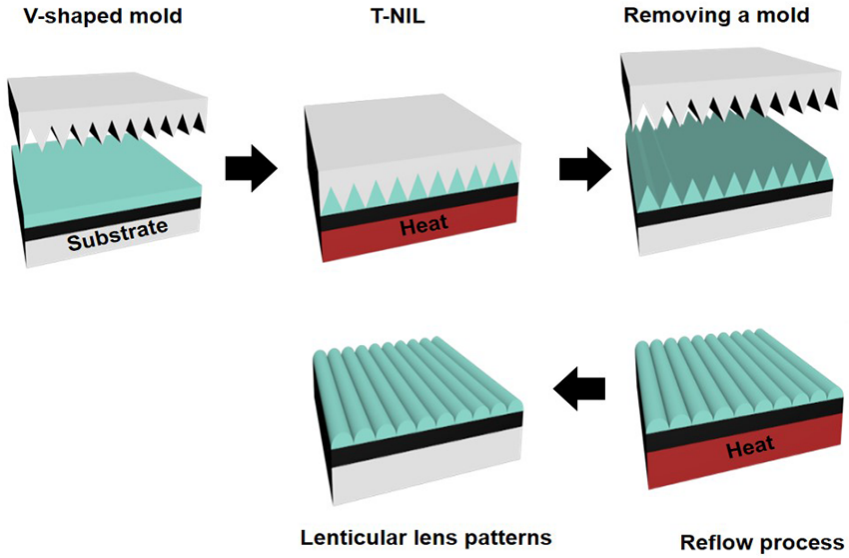

Fig. 1. A schematic illustration of the experimental procedure for fabricating a curved tunable microlens array.

Figure 1 shows a schematic illustration of the experimental process to fabricate curved structures such as a microlens array by thermal nanoimprint lithography and a successive thermal reflow process. First, we prepared a metallic V-shaped master by a micromachining method. After the preparation of a stainless steel block electroplated by nickel metal, the surface was mechanically machined by a diamond-cutting tool with desired angles and pitches. A V-shaped polydimethylsiloxane (PDMS) mold is obtained by filling a mixture of prepolymer and curing agent (with a ratio of 10:1) onto the nickel metal master and curing at 60°C for 3 hours followed by peeling off from the master. We used polystyrene (PS) to form the microlens pattern because it exhibits relatively strong adhesion to the substrate but strong antisticking properties to the PDMS [29,32]. A solution of PS (Mw: 2400, Yakuri Pure Chemicals Co., Ltd.) dissolved in toluene (Sigma-Aldrich) was spin-coated onto a silicon wafer substrate (1.5 cm × 1.5 cm) at 1000 rpm for 10 s. The solution concentration was varied between 10 and 20 wt% to control the thickness of the polymer films coated on the substrate. We placed the V-shaped PDMS mold onto the PS coated substrate and applied pressure (~4 bar), followed by increasing the substrate temperature to 150°C, which is above the T_g (55~70°C) of PS (Mw: 2100~2850) [33]. The detail experimental setup can be found elsewhere [31]. We note that viscosity shows the Arrhenius behavior on temperature explained Williams–Landel–Ferry (WLF) equation [34]. After heating for 15 minutes, we cooled the sample down to room temperature and detached the mold from the V-shaped PS patterns. After NIL, the thermal reflow process is used to fabricate rounded hemi-cylindrical patterns due to the surface energy minimization by heating it significantly above the Tg of PS

Optics EXPRESS

to lower the viscosity. In this work, we varied the reflow temperature (180~220°C) and duration time (10~20 min) for the thermal reflow process to optimize the conditions for fabricating microlens arrays.

3. Results and discussion

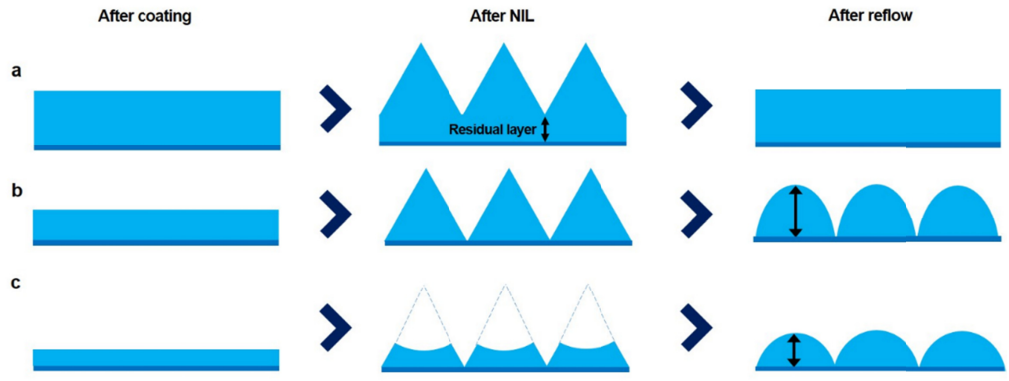

Fig. 2. Schematic representation of our concept of NIL by initial PS solution thickness and reflow process in appropriate conditions (a) when the initial PS thickness is thick, V-shaped patterns (width: 25 μm) after NIL are made with the residual layer. We assume that V-shaped patterns with the residual layer are flattened under the same reflow conditions compared with (b),(c) when the initial PS thickness for the residue-free state after NIL is perfect or insufficient, we presume lens shapes of different heights are formed after the reflow process.

Figure 2 shows the concept for the formation of a microlens array by NIL with the V-shaped mold and the reflow process at three different initial thickness ranges. When the initial polymer layer is thicker than a critical thickness, in which the polymer volume is the same as the void of the mold [30], the V-shaped patterns have a residual layer underneath after NIL, as shown in Fig. 2(a). In this experiment, we used a prism array with an angle of 40 degrees and a pitch of 25 μm, and the calculated critical polymer thickness is 5.24 μm. It is noted that we assumed that there is no density change during the NIL. Without the additional process of RIE to remove the residual layer, the polymeric structures flow down during the thermal reflow procedure when the temperature is slightly higher or the time of the reflow process is slightly longer than the optimized values. When the initial polymer thickness is exactly the same as the critical thickness, as shown in Fig. 2(b), there is no need to remove the residual layer ideally. However, if the thickness is higher than the critical value, even by a small amount, more than two polymeric structures can be merged even in a very thin residual layer between the structures. In the case of large-area fabrication, the uniformity of the temperature and the thickness should not be perfect, as the exact thickness is not suitable for the fabrication of a microlens in a large area [35]. When the polymer thickness is smaller than the critical value, the substrate is exposed by the dewetting of viscous polymer when the soft PDMS mold contacts the silicon oxide substrate [36]. It is noted that we choose PS due to its dewetting characteristics on the silicon oxide substrate, which have been studied in a few previous reports [37–39].

Optics EXPRESS

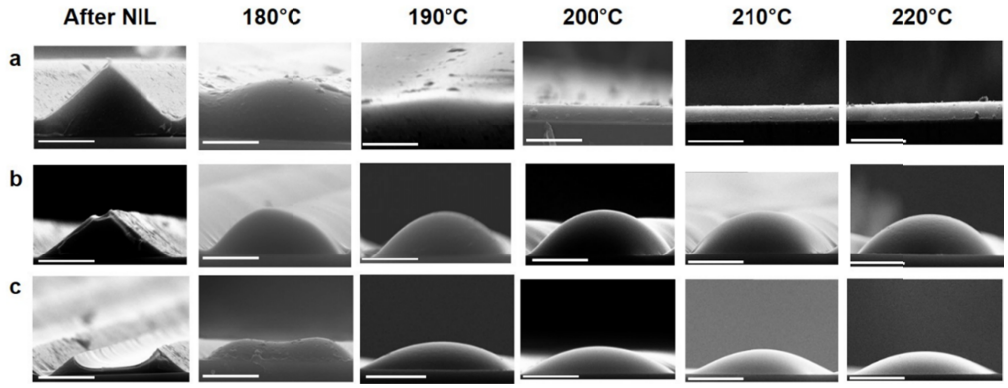

Fig. 3. Scanning microscopic (SEM) images (scale bar: 10 μm) of patterns imprinted with a V-shaped mold in three different thickness ranges. The leftmost panels represent the patterns produced by nanoimprinting and before thermal reflow. Images after the thermal reflow at different temperatures when the coating thickness is (a) 7.8 μm, (b) 4.2 μm, and (c) 1.9 μm.

Figure 3 shows experimental results that show the effect of temperature across a range of initial polymer thicknesses on the resulting lens shape by NIL and the reflow process. We perform the NIL with PS with different thicknesses of 7.8, 4.2 and 1.9 μm. Right after the NIL process without the thermal reflow step (shown in the left panel of Fig. 3), there is a residual layer when the coating thickness is 7.8 μm, and prism patterns are formed with a small void on the top when the thickness is 4.2 μm, which is thinner than the critical thickness. We vary the thermal reflow temperature from 180 to 220 °C while fixing the time to 10 minutes. As shown in Fig. 3(a), there is a slight reflow in the annealing at 180 °C, but it is flattened when the substrate temperature is higher than 200 °C. When the initial thickness is 4.2 and 1.9 μm, the V-shaped PDMS mold contacts the substrate without any residual layer. The NIL temperature (150 °C) is high enough to make the polymer viscous because a meniscus is formed on the surface of the wall of the PDMS mold. Interestingly, the viscous polymer melt is pinned on the edge of the substrate exposed by residue-free NIL during the thermal reflow process. Even under conditions of an annealing temperature higher than 220 °C, there is no flattening or merging of the prisms. The wide temperature range of the reflow process could be beneficial for a large-area fabrication, in which there are variations in the temperature on the hot plates. For an analysis of the self-pinning effect, we calculated the equilibrium contact angle by Young's equation [40].

$$\cos\theta = \frac{\gamma_{SiO2} - \gamma_{PS\text{-}SiO2}}{\gamma_{PS}} \tag{1}$$

where γ_{SiO2} and γ_{PS} are the surface tensions of the silicon oxide substrate and PS, and $\gamma_{PS-SiO2}$ is the interfacial tension between PS and SiO2. We obtain the interfacial tension by using the harmonic relation of the dispersion and polar components of the surface tensions as below [32].

$$\gamma_{PS\text{-}SiO2} = \gamma_{PS} + \gamma_{SiO2} - \frac{4\gamma_{PS}^{d}\gamma_{SiO2}^{d}}{\gamma_{PS}^{d} + \gamma_{SiO2}^{d}} - \frac{4\gamma_{PS}^{p}\gamma_{SiO2}^{p}}{\gamma_{PS}^{p} + \gamma_{SiO2}^{p}} \tag{2}$$

where γ^{d} and γ^{p} are the dispersion and polar components of the surface tensions of PS and SiO_2, respectively. We use the data from a reference [40], γ_{PS}^{d} = 33.9, γ_{PS}^{p} = 6.8, γ_{SiO2}^{d} = 23, γ_{SiO2}^{p} = 35 mN/m, and calculate the interfacial tension to be 21 mN/m and the equilibrium contact angle to be 24.6°. From Fig. 3(b), the 52° angle of the hemisphere is higher than the

Optics EXPRESS

equilibrium angle in the high polymer thickness regime, which means that the polymer melts could spread to be flattened when the annealing time is long enough. On the other hand, when the lens angle is 22°, smaller than the equilibrium value from Fig. 3(c), there can be an additional dewetting of polymer melts to form the equilibrium contact angle.

In this experiment, the self-pinning effect is strong enough to fix the boundary not to dewet or spread in the temperature range of 180 ~220 °C, which is a reasonable range in a large area fabrication. Additionally, we can tune the hemispherical shape by controlling the coated polymer thickness, as shown in Fig. 3(b) and 3(c). We note the self-pinning process is also from the residue free process because the oxygen plasma etching to remove the residual layer activates the substrate surface to spread the polymer melt to be flattened during thermal reflow. In addition, the lens formation process can be used in different geometries or dimensions as shown in Fig. 4. Figure 4(a) shows a lenticular lens array with a pitch of 10 μm. As shown in Fig. 4(b), we obtain two dimensional lens array after reflow followed by nanoimprint lithography by a pyramidal stamp.

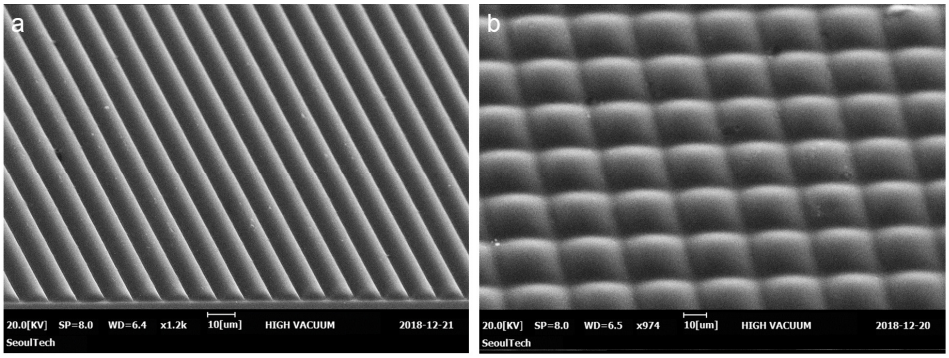

Fig. 4. SEM images of (a) a lenticular lens array (pitch: 10 μm) and (b) a two-dimensional lens array.

Figure 5 shows the lens shape modulation by the control of the coating thickness. The images in the left panel are SEM images after nanoimprint lithography. When the coating thickness is 1.9 μm, the imprinted pattern has a V-shape with a large void in the apex area of the prism. In the case of a 1.9-μm, no residual layer is formed between the polymeric structures. After a reflow process at 200 °C for 10 min, the V-shaped structure takes on a rounded lens shape to minimize the surface area. The contact angle of the lens is approximately 23°, which is measured from the SEM image. When the coating thickness is increased from 1.9 μm to 4.2 μm, which is still smaller than the critical thickness (5.2 μm with the prism mold), the contact angle of the lens is increased from 22° to 53°.

To estimate the relation between the focal length and coating thicknesses, we establish the relevant equations below by using a mass balance before the nanoimprint lithography and after the reflow process followed by nanoimprint.

$$Lt = \frac{1}{2}R^2(\theta - \sin 2\theta),\ 2R\sin\theta = L \tag{3}$$

where L is the diameter of the lens or the period of the lens array, t is the coating thickness, R is the radius of curvature of the lens and θ is the contact angle, as defined in Fig. 6(a). The mass is assumed to be conserved after the nanoimprinting without the residue removal process. As shown in Fig. 6(b), the contact angle calculated from Eq. (3) is in agreement with the experimental data. Based on such a simple model using a mass balance, one can estimate the curvature and the shape of the lens depending on the initial thickness of the coated

Optics EXPRESS

polymer film. Figure 6(c) shows the optical simulation results on the focal lengths from PS lenses (refractive index: 1.59) in different curvatures (COMSOL Multiphysics). When the coating thickness is decreased, the focal length is increased. Also, the focal length (f) of the lens can be calculated as below [41].

$$f = \frac{R}{n - 1} \tag{4}$$

Where n is the refractive index of materials used in making microlens arrays. Figure 6(d) shows the graph showing the relation between focal length and coating thickness. From the Eq. (4) and the simulation data, the focal length can be modulated by the initial coating thickness and the refractive index which can be changed by replica molding methods.

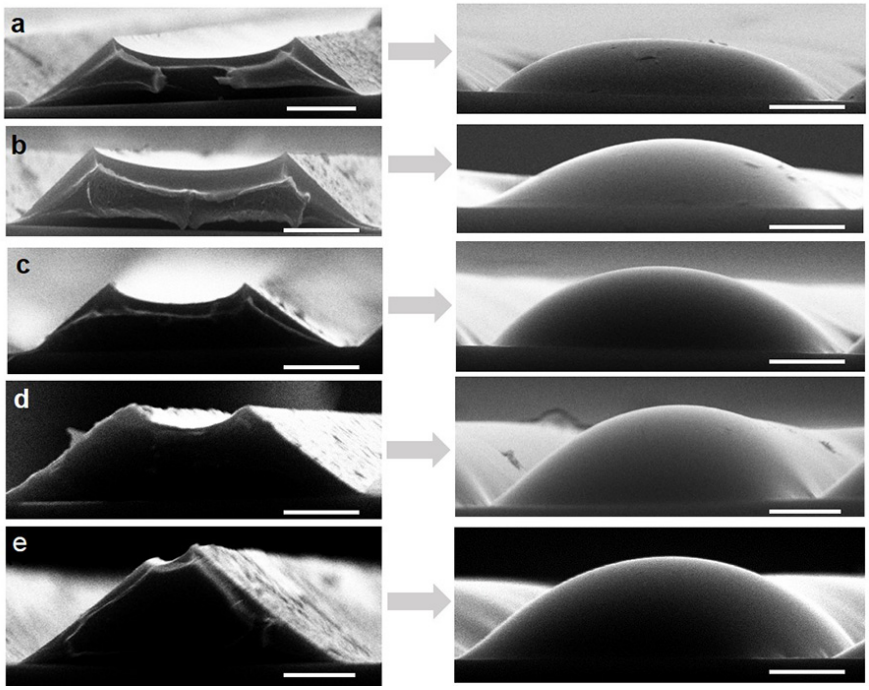

Fig. 5. SEM images of lens shapes with different curvatures with the control of the initial thickness at (a) 1.9 μm, (b) 2.4 μm, (c) 3.7 μm, (d) 4.1 μm, and (e) 4.2 μm. The left and right panels represent the SEM images before and after the thermal reflow (for 10 min at 200 °C), respectively. (Scale bar: 5 μm)

Optics EXPRESS

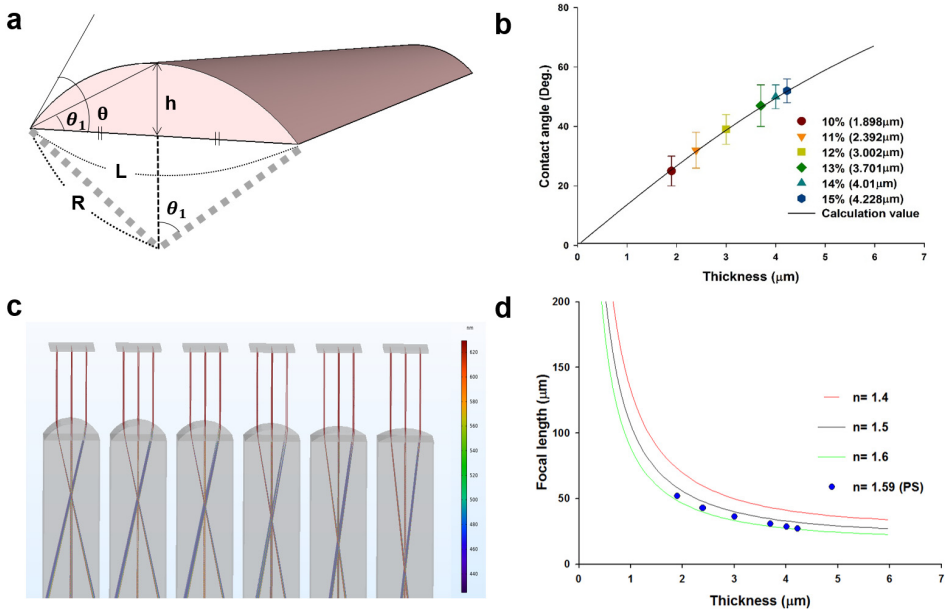

Fig. 6. (a) Schematic images showing the mass balance before and after the process. Graphs showing the relation of (b) coating thickness versus contact angle, (c) optical simulation results on focal lengths of lenses, (d) coating thickness versus focal length from Eq. (4) and optical simulation.

4. Conclusion

We proposed the fabrication of a lens array in a wide range by using the self-pinning effect on the three-phase contact lines between the polymer-air-substrate. By using the pinning effect, we can obtain a large window for the thermal reflow to form a lens array. We exploit a V-shaped mold to expose the surface to remove the residual layer after the nanoimprint lithograph, which is essential to reduce the post process such as oxygen plasma etching and hydrophobic treatment to enhance the pinning effect. In addition, we control the thickness to manipulate the focal length of the lens. The new method to fabricate the lens array by using residue-free nanoimprint lithography with a V-shaped mold can be used for large-area fabrication because the temperature range is wide and there is no need to use equipment under a high-vacuum condition.

Funding

National Research Foundation of Korea (NRF); Program (2016R1A2B4013640); Commercializations Promotion Agency for R&D Outcomes; Program (2018000145).

References

1. Y. Fu and B. K. A. Ngoi, "Investigation of diffractive-refractive microlens array fabricated by focused ion beam technology," Opt. Eng. **40**(4), 511–517 (2001).
2. J. Long-Wen, H. Yin-Lei, W. Yan, Q. Bing, and Z. Wen-xing, "Preparation of a self-focusing lens for optical communication," Optics and Precision Engineering **5**, 012 (2002).
3. H. Ren, Y.-H. Fan, Y.-H. Lin, and S.-T. Wu, "Tunable-focus microlens arrays using nanosized polymer-dispersed liquid crystal droplets," Opt. Commun. **247**(1-3), 101–106 (2005).
4. P. Dannberg, L. Erdmann, R. Bierbaum, A. Krehl, A. Bräuer, and E. B. Kley, "Micro-optical elements and their integration to glass and optoelectronic wafers," Microsyst. Technol. **6**, 41–47 (1999).
5. W.-K. Choi, S.-H. Kim, and E.-S. Lee, "Electrochemical micro machining characteristics of Fe 64 Ni 36 invar film using micro WC rod electrode," Microsyst. Technol. **23**(2), 405–410 (2017).

Optics EXPRESS

6. S. James and A. Sonate, "Experimental study on micromachining of CFRP/Ti stacks using micro ultrasonic machining process," Int. J. Adv. Manuf. Tech. **95**(1-4), 1539–1547 (2018).
7. L. Li, W. Nie, Z. Li, Q. Lu, C. Romero, J. R. Vázquez de Aldana, and F. Chen, "All-laser-micromachining of ridge waveguides in $LiNbO_3$ crystal for mid-infrared band applications," Sci. Rep. **7**(1), 7034 (2017).
8. H. He, N. Qu, Y. Zeng, and Y. Yao, "Enhancement of mass transport in wire electrochemical micro-machining by using a micro-wire with surface microstructures," Int. J. Adv. Manuf. Tech. **89**(9-12), 3177–3186 (2017).
9. V. Rathod, B. Doloi, and B. Bhattacharyya, "Fabrication of microgrooves with varied cross-sections by electrochemical micromachining," Int. J. Adv. Manuf. Tech. **92**(1-4), 505–518 (2017).
10. C. S. Lau, C. Khor, D. Soares, J. Teixeira, and M. Abdullah, "Thermo-mechanical challenges of reflowed lead-free solder joints in surface mount components: a review," Solder. Surf. Mt. Technol. **28**(2), 41–62 (2016).
11. S.-I. Chang and J.-B. Yoon, "Shape-controlled, high fill-factor microlens arrays fabricated by a 3D diffuser lithography and plastic replication method," Opt. Express **12**(25), 6366–6371 (2004).
12. H. Schift, C. Spreu, A. Schleunitz, and J. J. Lee, "Shape control of polymer reflow structures fabricated by nanoimprint lithography," Microelectron. Eng. **88**(1), 87–92 (2011).
13. C. Peng, X. Liang, Z. Fu, and S. Y. Chou, "High fidelity fabrication of microlens arrays by nanoimprint using conformal mold duplication and low-pressure liquid material curing," J. Vac. Sci. Technol. B **25**(2), 410 (2007).
14. E. Rognin, S. Landis, and L. Davoust, "Dewetting of the residual layer of annealed nanoimprinted polystyrene films," Microelectron. Eng. **141**, 198–202 (2015).
15. A. Schleunitz, C. Spreu, M. Vogler, H. Atasoy, and H. Schift, "Combining nanoimprint lithography and a molecular weight selective thermal reflow for the generation of mixed 3D structures," J. Vac. Sci. Technol. B **29**(6), 06FC01 (2011).
16. J. J. Chae, S. H. Lee, and K. Y. Suh, "Fabrication of Multiscale Gradient Polymer Patterns by Direct Molding and Spatially Controlled Reflow," Adv. Funct. Mater. **21**(6), 1147–1153 (2010).
17. K. Ishihara, M. Fujita, I. Matsubara, T. Asano, S. Noda, H. Ohata, A. Hirasawa, H. Nakada, and N. Shimoji, "Organic light-emitting diodes with photonic crystals on glass substrate fabricated by nanoimprint lithography," Appl. Phys. Lett. **90**(11), 111114 (2007).
18. T. Senn, J. Bischoff, N. Nüsse, M. Schoengen, and B. Löchel, "Fabrication of photonic crystals for applications in the visible range by nanoimprint lithography," Photon. Nanostructures **9**(3), 248–254 (2011).
19. J. L. Charest, M. T. Eliason, A. J. García, and W. P. King, "Combined microscale mechanical topography and chemical patterns on polymer cell culture substrates," Biomaterials **27**(11), 2487–2494 (2006).
20. W. Hu, E. K. Yim, R. M. Reano, K. W. Leong, and S. W. Pang, "Effects of nanoimprinted patterns in tissue-culture polystyrene on cell behavior," J. Vac. Sci. Technol. A **23**(6), 2984–2989 (2005).
21. K. Sakoda and M. Van de Voorde, *Micro-and Nanophotonic Technologies* (John Wiley & Sons, 2017).
22. M. D. Austin and S. Y. Chou, "Fabrication of 70 nm channel length polymer organic thin-film transistors using nanoimprint lithography," Appl. Phys. Lett. **81**(23), 4431–4433 (2002).
23. S. H. Kim, K.-D. Lee, J.-Y. Kim, M.-K. Kwon, and S.-J. Park, "Fabrication of photonic crystal structures on light emitting diodes by nanoimprint lithography," Nanotechnology **18**(5), 055306 (2007).
24. M. Li, H. Tan, L. Chen, J. Wang, and S. Y. Chou, "Large area direct nanoimprinting of SiO_2–TiO_2 gel gratings for optical applications," J. Vac. Sci. Technol. B Microelectron. Nanometer Struct. Process. Meas. Phenom. **21**(2), 660–663 (2003).
25. J. Zhang, L. Zhang, L. Han, Z.-W. Tian, Z.-Q. Tian, and D. Zhan, "Electrochemical nanoimprint lithography: when nanoimprint lithography meets metal assisted chemical etching," Nanoscale **9**(22), 7476–7482 (2017).
26. Y. H. Kang, J. H. Han, S. Y. Cho, and C.-G. Choi, "Resist-free antireflective nanostructured film fabricated by thermal-NIL," Nano Converg. **1**(1), 19 (2014).
27. I. Zadorozhnyi, J. Li, S. Pud, M. Petrychuk, and S. Vitusevich, "Single-trap kinetic in Si nanowire FETs: effect of gamma radiation treatment," MRS Adv. **1**(56), 3755–3760 (2016).
28. J. G. Ok, Y. J. Shin, H. J. Park, and L. J. Guo, "A step toward next-generation nanoimprint lithography: extending productivity and applicability," Appl. Phys., A Mater. Sci. Process. **121**(2), 343–356 (2015).
29. H. Schift, "Nanoimprint lithography: An old story in modern times? A review," J. Vac. Sci. Technol. B **26**(2), 458–480 (2008).
30. H. Yoon, H. Lee, and W. B. Lee, "Toward residual-layer-free nanoimprint lithography in large-area fabrication," Korea-Aust. Rheol. J. **26**, 39–48 (2014).
31. H. Yoon, K. M. Lee, D. Y. Khang, H. H. Lee, and S. J. Choi, "Rapid flash patterning of nanostructures," Appl. Phys. Lett. **85**(10), 1793–1795 (2004).
32. C. Acikgoz, M. A. Hempenius, J. Huskens, and G. J. Vancso, "Polymers in conventional and alternative lithography for the fabrication of nanostructures," Eur. Polym. J. **47**(11), 2033–2052 (2011).
33. R. Claudy, J. M. Létoffé, Y. Camberlain, and J. R. Pascault, "Glass Transition of Polystyrene Versus Molecular Weight," Polym. Bull. **9**, 208–215 (1983).
34. H. C. Scheer, N. Bogdanski, M. Wissen, and S. Mollenbeck, "Imprintability of polymers for thermal nanoimprint," Microelectron. Eng. **85**(5-6), 890–896 (2008).
35. H.-K. Lee, S.-I. Chang, and E. Yoon, "A flexible polymer tactile sensor: Fabrication and modular expandability for large area deployment," J. Microelectromech. Syst. **15**(6), 1681–1686 (2006).
36. H.-L. Zhang, D. G. Bucknall, and A. Dupuis, "Uniform nanoscopic polystyrene patterns produced from a microscopic mold," Nano Lett. **4**(8), 1513–1519 (2004).

Optics EXPRESS

37. B. Radha and G. U. Kulkarni, "Dewetting assisted patterning of polystyrene by soft lithography to create nanotrenches for nanomaterial deposition," ACS Appl. Mater. Interfaces **1**(2), 257–260 (2009).
38. J. Becker, G. Grün, R. Seemann, H. Mantz, K. Jacobs, K. R. Mecke, and R. Blossey, "Complex dewetting scenarios captured by thin-film models," Nat. Mater. **2**(1), 59–63 (2003).
39. J. Peng, R. Xing, Y. Wu, B. Li, Y. Han, W. Knoll, and D. H. Kim, "Dewetting of thin polystyrene films under confinement," Langmuir **23**(5), 2326–2329 (2007).
40. J. Brandrup, E. H. Immergut, E. A. Grulke, A. Abe, and D. R. Bloch, *Polymer handbook. 3rd edn*, (Wiley New York etc, 1989).
41. Q. Xu, B. Dai, Y. Huang, H. Wang, Z. Yang, K. Wang, S. Zhuang, and D. Zhang, "Fabrication of polymer microlens array with controllable focal length by modifying surface wettability," Opt. Express **26**(4), 4172–4182 (2018).